Research Article

Chemical Review and Letters
journal homepage: www.chemrevlett.com
ISSN (online): 2645-4947 (print) 2676-7279

Effective removal of cefixime and amoxicillin from aqueous solutions using ZnO/Fe_3O_4@GO magnetic nanocomposites

Seyyed Komeil Hosseini Sfandani[1], Hamid Reza Ghorbani[1,*], Fatemeh Ardestani[1], Mehri Esfahanian[1] and Zinatossadat Hossaini[2]

[1]*Department of Chemical Engineering, Qaemshahr Branch, Islamic Azad University, Qaemshahr, Iran*
[2]*Department of Chemistry, Qaemshahr Branch, Islamic Azad University, Qaemshahr, Iran*

ARTICLE INFO

Article history:
Received 12 July 2024
Received in revised form 07 October 2024
Accepted 08 October 2024
Available online 15 October 2024

Keywords:
ZnO/Fe_3O_4@GO
Adsorption isotherm
Amoxiciline
Cefixime

ABSTRACT

The water extract of *Petasits hybridus* leaves was used in this study to create the high-performance ZnO/Fe_3O_4@GO magnetic nanocomposites, which were then used as an environmentally friendly adsorbent for the removal of amoxicillin (AMX) and cefixime (CFX). The initial concentrations of CFX and AMX, contact time, solution pH, temperature, and adsorbent dose were among the adsorption parameters that were examined. The pseudo second-order and Langmuir models, respectively, provided good fits to the adsorption kinetic and isotherm. When CFX and AMX are adsorbed onto ZnO/Fe_3O_4@GO nanocomposite, the initial amounts are 10 mg. Moreover, ZnO/Fe_3O_4@GO adsorb CFX and AMX at pH values of 6 and 8.5 respectively. The low cost of the adsorbent, its great efficiency, and its ease of use are its advantages.

1. Introduction

Due to their significance in medical treatment, numerous antibiotic compounds serve a variety of purposes. However, the pharmaceutical business, veterinary medicine, and human medicine frequently face challenges related to their aquatic environment [1]. In the human or animal body, between 30 and 90 percent of the administered dose would remain indegradable and be primarily eliminated as the active ingredient [2, 3]. Even with waste treatment, at least half of the medications contain antibiotics, including ampicillin, erythromycin, sulfamethoxazole, tetracycline, and penicilloyl, which are extremely harmful to the environment when used continuously [4]. Numerous pesticides are hazardous to algae and other low-level organisms, according to recent studies, which can have an immediate impact on ecological sustainability over the long run [5-7]. Because of the increasing population and widespread use of chemicals, water pollution is becoming a more significant issue on a global scale. Pharmaceutical chemicals, especially antibiotics, are regarded as environmentally major issues among the different contaminants [8–10]. Antibiotics are a class of medications that are widely used in both human and veterinary care to prevent and treat disease. They are primarily introduced into the aquatic environment through agricultural runoff, veterinary clinics, and human waste [11–13]. A semi-synthetic substance, cefixime (CFX) is typically categorized as a third-generation cephalosporin. Numerous bacterial and infectious illnesses, including lung infections, infections of the skin and soft tissues, infections of the bones or joints, and urinary tract infections, can be effectively treated with CFX. In patients having surgery or those who are prone to infections for any other cause, it can also be used to prevent infections [14–16].

However, between 40 and 50 percent of the CFX that is consumed is not broken down and is instead eliminated unaltered through human urine.

* Corresponding author; e-mail: hamidghorbani6@gmail.com
https://doi.org/10.22034/crl.2024.467458.1375

As a result, CFX can reach the environment in a number of ways, such as through hospital effluents, household wastewater, emissions from industrial antibiotic producers, and other sources, either unaltered or as their metabolites. Antibiotic-resistant microbes will evolve as a result of this antibiotic's non-biodegradable nature, even at low environmental concentrations [17].

Advanced oxidation, photocatalytic degradation, coagulation-flocculation, membrane filtration, electrolysis, and adsorption are some of the treatment technologies that have been employed thus far to remove CFX from wastewater. Adsorption is cost-effective and efficient [18,19]. A broad-spectrum beta-lactam antibiotic, amoxicillin is a member of the penicillin class and is used in veterinary medicine to treat bacterial infections that occur in the gastrointestinal tract and throughout the body [20]. Because of its wide range of antibacterial properties, it is also frequently used as a therapeutic agent and in human prescription medication (against bacterial infections) [21].

Additionally, amoxicillin has been found to be barely biodegradable and to remain an active ingredient in feces and urine [22, 23]. Furthermore, the concentration of amoxicillin that accumulates through the industrial route is typically far larger than that which originates from public excretion. Some possible future issues may be linked to their presence in the environment. Pan et al., for instance, have documented the compound's harmful effects on the algae Synechocystis sp., mostly through blocking its photosynthetic mechanism. Additionally, amoxicillin would raise the resistance of dangerous bacteria when it accumulated within a single organism, requiring a higher dosage or possibly rendering it incapable of treating typical infections. There are numerous eco-friendly coatings available nowadays. One-dimensional macromolecules with exceptional chemical stability and heat resistance include carbon nanotubes (CNTs). CNT has unique uses in a number of domains, including nanotechnology and biosensors [24].

Magnetic nanostructures, characterized by high surface area, superparamagnetism, and biocompatibility, find diverse applications in adsorption, catalytic synthesis, and medicine. Their potential is further expanded through ongoing research into synthesis and functionalization [25]. In heterogeneous Fenton-like processes, graphene oxide (GO) enhances the catalytic activity of nanoparticles by serving as an effective support, leveraging its extensive surface area and favorable properties for pollutant removal.

Additionally, the current study investigated the utilization of Petasites hybridus rhizome water extract as a novel adsorbent for the removal of CFX and AMX from water in order to prepare a ZnO/Fe_3O_4@GO nanocomposite. The empirical factors, which included the initial concentration of CFX and AMX, the adsorbent dosage, and the pH of the CFX, AMX, and adsorbent solutions, were then examined.

The adsorption of CFX onto ZnO/Fe_3O_4@GO was eventually studied using isotherms. Another study examines ZnO/Fe_3O_4@GO as a novel and affordable sorbent for the removal of amoxicillin and cefixime, two aromatic heterocyclic antibiotics (Figure 1) [26-30].

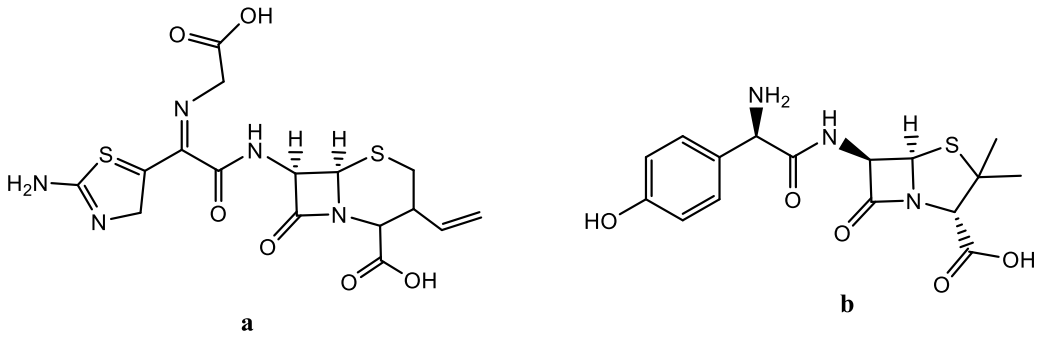

Fig. 1. The structure of a) Cefixime and b) Amoxicillin

2. Results and discussion

ZnO/Fe_3O_4@GO nanocomposites were made in this study using the co-precipitation technique. The structure of produced ZnO/Fe_3O_4@GO nanocomposites was confirmed by a number of investigations, including FT-IR, XRD, VSM, SEM–EDX, TEM, and TGA study. The rhizome water extract of Petasites hybridus was used to create the ZnO/Fe_3O_4@GO. To determine and confirm the creation of ZnO/Fe_3O_4@GO, we used the scanning electron microscopy (SEM) approach (Figure 2). Additionally, we calculated the particle size of

ZnO/Fe_3O_4@GO MNCs using the X-ray diffraction patterns (XRD) method (Figure 3). The Debye-Scherrer

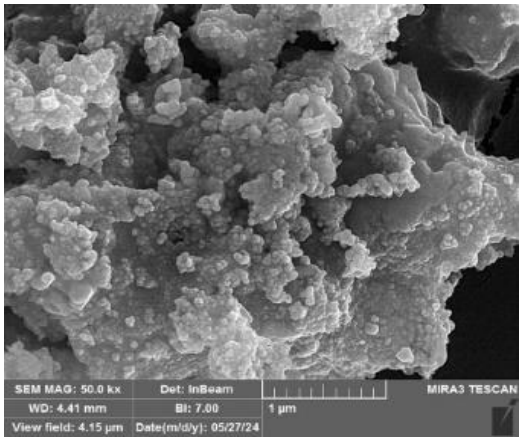

Fig. 2. SEM image of ZnO/Fe_3O_4@GO MNCs

equation ($D=K\lambda/\beta\cos\theta$) has been used to determine that the size of the ZnO/Fe_3O_4@GO MNCs particles is 33.8 nm. After the fifth reusability, we are provided the catalyst's XRD and IR to confirm its reusability. After seven cycles, all of the XRD peaks stayed at the same levels, indicating that the crystalline structure has not changed.

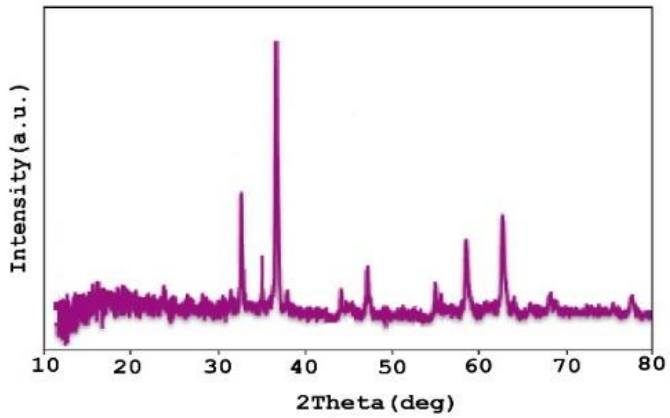

Fig. 3. XRD of ZnO/Fe_3O_4@GO MNCs

Additionally, the detected peaks are in good agreement with the JCPDS card no. 01-0646 and appear at 2θ approximately 25.2° and 43.6°, which correspond to the usual structure of GO. The end result is a complex of Fe_3O_4, ZnO, and GO, as evidenced by the ZnO/Fe_3O_4@GO MNPs peaks, which are comparatively weaker than those of the pure materials but match the ZnO and Fe_3O_4 XRD patterns well. Furthermore, significant crystallinity is shown by the nanocomposite's strong diffraction peaks. Using the EDX method, an elemental analysis of the produced ZnO/Fe_3O_4@GO MNPs was performed (Figure 4). The Zn, Fe, C and O peaks of ZnO/Fe_3O_4@GO MNPs showed successful preparation, as shown in Figure 4. Additionally, the presence of a carbon peak in the EDX spectrum suggests the presence of nanoscale organic molecules.

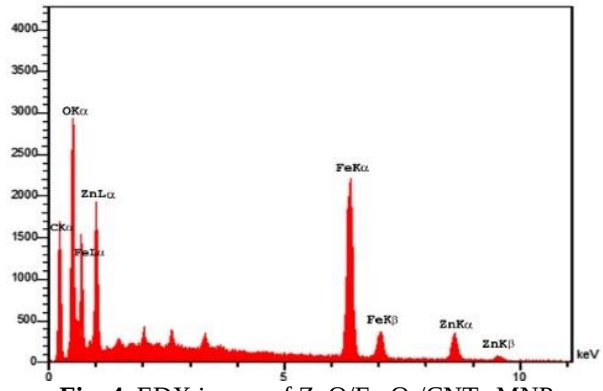

Fig. 4. EDX image of ZnO/Fe_3O_4/CNTs MNPs

As seen in Figure 5, the samples were examined using TEM in order to acquire a clear size, shape, and structural image of the ZnO/Fe_3O_4@GO MNCs. It is evident that the GO supports ZnO/Fe_3O_4@GO. The saturation magnetization (Ms) values of the pure Fe_3O_4 MNPs and magnetic ZnO/Fe_3O_4@GO MNCs are displayed in Figure 5. Each sample showed normal superparamagnetic characteristics with very little remanence or coercivity. The Ms of the ZnO/Fe_3O_4@GO MNCs (31.6 emu/g) was significantly lower than that of pure Fe_3O_4 NPs (59.8 emu/g), as shown in Figure 5.

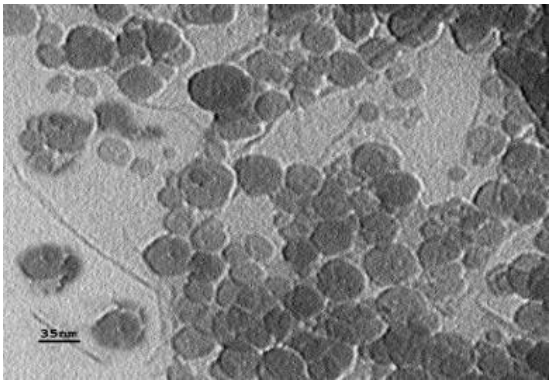

Fig. 5. TEM image of the Fe_3O_4/ZnO/GO MNCs

Brunauer–Emmett–Teller (BET) adsorption isotherm analysis

By analyzing the adsorption isotherms of nitrogen on the surface of the ZnO/Fe3O4@GO MNCs nanocomposites at increasing relative pressure, the BET surface area, pore size and volume were determined (Figure 6). The pore structure of the ZnO/Fe3O4@GO MNCs nanocomposite sample was investigated by nitrogen adsorption–desorption isotherms and the pore size distribution were calculated by BJH method according to the desorption

branch. It is well known that when size of the catalyst will decrease, the surface area will be increased, the same trend has been observed in this work, which is confirmed by BET analysis as shown in Table 1.

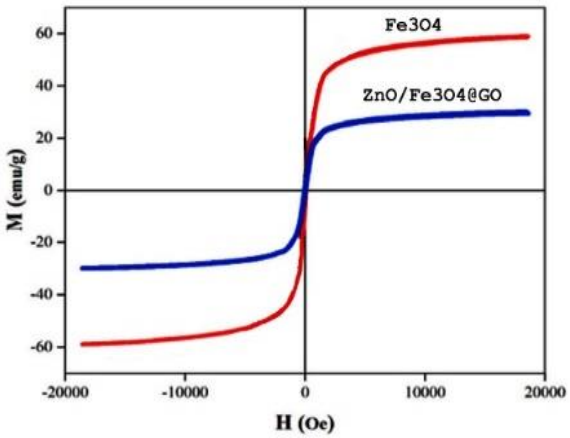

Fig. 5. VSM analysis of ZnO/Fe_3O_4@GO MNCs

The ternary ZnO/Fe_3O_4@GO MNCs nanocomposite shows highest surface area (Table 1) compared with binary nanocomposites ZnO, Fe_3O_4 and ZnO/Fe_3O_4. The difference in their surface area was due to the synergetic effect among the components such as ZnO, Fe_3O_4 and GO in the composite system. The increase in the surface area was significant; hence, the larger surface area of ZnO/Fe_3O_4@GO MNCs nanocomposite will benefit the spatial separation of redox sites in the crystals which can enhance electron-transfer properties of the nanocomposite.

Effect of pH

Because the pH can alter adsorption routes, the solution pH of CFX and AMX in the bath system is a crucial parameter that can influence the adsorption of CFX and AMX on the ZnO/Fe_3O_4@GO MNCs.

Table 1. BET data of the synthesized ZnO/Fe_3O_4@GO

Catalysts	Surface area BET (m^2/g)	Pore Volume (cm^3/g)	Pore diameter (nm)
GO	235.6247	0.7248	16.6528
ZnO	15.7845	0.04725	35.7457
ZnO/Fe_3O_4	21.04576	0.10047	30.7128
Fe_3O_4	12.5478	0.40175	21.4752
ZnO/Fe_3O_4@GO MNCs	134.7824	0.58745	15.3247

Therefore, CFX and AMX were eliminated using bath tests conducted in the range of 1 to 10 with the initial concentrations of CFX and AMX fixed at 10 mgL^{-1} and 5 mg of ZnO/Fe_3O_4@GO MNCs. As the pH of the solution rises from 1 to 10, as shown in Figure 6, the adsorption effectiveness of CFX improves from 65.2% to 98.5%, with the highest adsorption for CFX occurring at pH=6. Additionally, as the pH of the solution rises from 1 to 10, the AMX adsorption effectiveness increases from 73.5% to 97.5%, with the greatest adsorption for AMX occurring at pH=8.5. The ZnO/Fe_3O_4@GO MNCs surface charge and the degree of ionization of the CFX and AMX could account for the effect of solution pH.

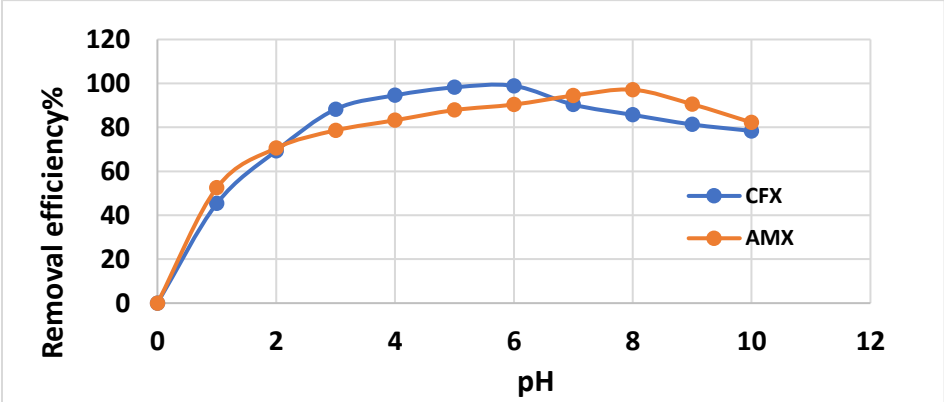

Fig. 6. Effect of pH on the adsorption of CFX and AMX

The amount of ZnO/Fe_3O_4@GO nanocomposite

One of the most important aspects influencing the ZnO/Fe_3O_4@GO MNCs capability for an initial concentration of the CFX and AMX is the amount of ZnO/Fe_3O_4@GO nanocomposite. To get the ideal amount of ZnO/Fe_3O_4@GO MNCs while maintaining other empirical parameters constant, different doses of the nanocomposite (ranging from 2 to 20 mg) were used with an initial concentration of 10 mg L^{-1} CFX and AMX (Figure 7). With an increase in ZnO/Fe_3O_4@GO MNCs from 2 to 20 mg, the removal of CFX and AMX employing this nanocomposite rose from 65.32% to 97.8% and 64.32% to 99.2% with 8 mg and 10 mg of ZnO/Fe_3O_4@GO MNCs, respectively, the adsorption of CFX and AMX reached its maximum level. It may have something to do with the improvement of accessible active sites on the ZnO/Fe_3O_4@GO MNCs surface. Initially, the entire surface of the ZnO/Fe_3O_4@GO MNCs is completely exposed, which can promote CFX and AMX ion approachability to a vast array of the active sites on the ZnO/Fe_3O_4@GO MNCs. Following that, the qe becomes stable even if the amount of ZnO/Fe_3O_4@GO MNCs increases to 8 and 10 mg.

Effect of initial CFX and AMX Concentration

Another important factor affecting bath efficiency is initial concentration. In order to investigate the impact of starting concentrations of CFX and AMX on the adsorption of these compounds *via* the ZnO/Fe_3O_4@GO, the initial concentration ranges were 10 to 60 mg L^{-1} (Figure 8). The adsorption efficiency of CFX and AMX decreased with the increase of initial concentration in the first stage, reaching minimal values at higher concentrations, as illustrated in Figure 8, as the starting concentrations of both substances increased from 10 to 60 mg L^{-1}. Additionally, the result indicates that adsorption capacities (q_e) increase rapidly as the initial concentration (c_e) increases. This is because the ZnO/Fe_3O_4@GO has a large number of accessible active positions, and the growth rate of qe slowed down at higher initial concentrations because the number of active positions on the ZnO/Fe_3O_4@GO was fixed.

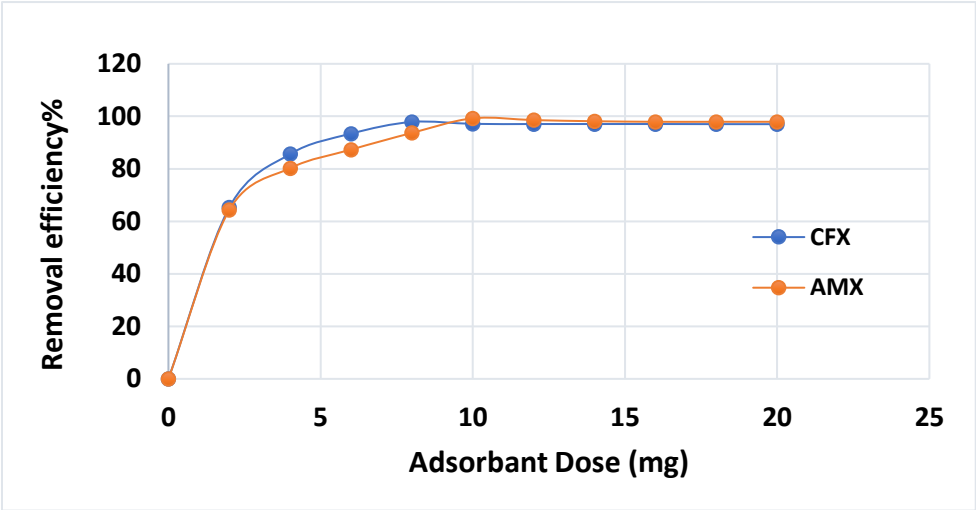

Fig. 7. Effect of adsorbent dose on the adsorption of CFX and AMX

Adsorption isotherms

In this section, to enhance the understanding of the adsorption mechanism of, for instance, CFX onto ZnO/Fe_3O_4@GO, it is imperative to investigate the equilibrium isotherm. To this end, the equilibrium adsorption of CFX onto the surface of ZnO/Fe_3O_4@GO was scrutinized utilizing the linear representation of two-parameter models, namely Langmuir (L) and Freundlich (F). The Langmuir model posits that a monolayer adsorption of CFX transpires on the surface of the ZnO/Fe_3O_4@GO, wherein all adsorption sites are considered equivalent, which can be expressed as Equation 1:

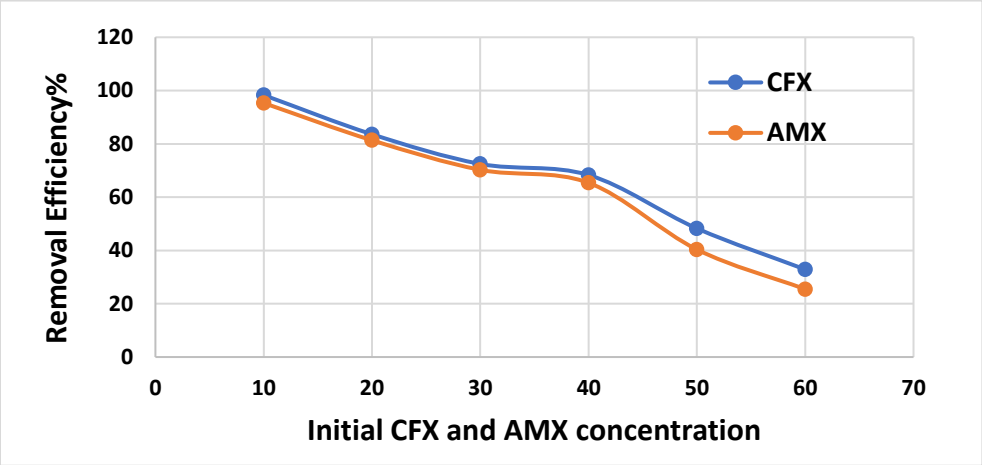

Fig. 8. Effect of initial CFX and AMX concentration on the adsorption

$$\frac{C_e}{q_e} = \frac{C_e}{q_m} + \frac{1}{q_m^{b1}} \quad (1)$$

Where q_e (mgg^{-1}) and C_e (mgL^{-1}) denote the concentrations of adsorbed CFX onto ZnO/Fe_3O_4@GO and in the aqueous phase, respectively, qm (mgg^{-1}) characterizes the maximum adsorption capacity of ZnO/Fe_3O_4@GO for CFX. The Freundlich model posits that multilayer adsorption of CFX transpires on the surface of ZnO/Fe_3O_4@GO, with adsorption sites exhibiting heterogeneous accessibility and varying adsorption energies. The linear representation of the Freundlich equation can be articulated as Equation 2:

$$\ln q_e = \frac{1}{n}\ln c_e + \ln k_f \quad (2)$$

where k_f ($mg^{1-(1/n)}\, l^{1/n}\, g^{-1}$) depicts fixed of F and n appears the heterogeneity of adsorption.The parameters pertaining to the Langmuir (L) and Freundlich (F) models for the adsorption of CFX onto the ZnO/Fe_3O_4@GO composite are delineated in Table 2, while the linear regression analyses of these models are graphically represented in Figure 11. The coefficient of determination (r^2) values for the L and F models were determined to be 0.9928 and 0.9651, respectively. The Langmuir model postulates that the adsorption process occurs in a monolayer fashion on the surface of the ZnO/Fe_3O_4@GO, characterized by a finite number of identical adsorption sites that are energetically uniform, and posits that there is an absence of interactions among the adsorbed CFX molecules. Furthermore, this finding suggests that the adsorption of CFX onto ZnO/Fe_3O_4@GO occurs through heterogeneous binding sites. The maximum adsorption capacity (qmax) of CFX on ZnO/Fe_3O_4@GO was quantified to be 275.3 $mg\ g^{-1}$.

Table 2. Obtained parameters for adsorption of CFX onto Fe_3O_4/ZnO@GO

Isotherm	Parameters	Values	R^2
L	q_m($mg\ g^{-1}$)	275.3	0.9928
	K_L	0.852	
F	k_f ($mg^{1-(1/n)}\, l^{1/n}\, g^{-1}$)	142.3	0.9651
	n	4.32	

3. Experimental

Materials and methods

General

The Petasites hybridus were purchased from Mazandaran, Babol and used as green media for the synthesis of magnetic nanocomposite. All materials employed in this work were purchased from Fluka and Merck with no further purification. The structure of Fe_3O_4/ZnO@GO was confirmed by XRD, SEM, EDX and. X-ray diffraction patterns (XRD) were performed for calculating of the size of prepared Fe_3O_4/ZnO@GO. The Scherrer's formula; D=

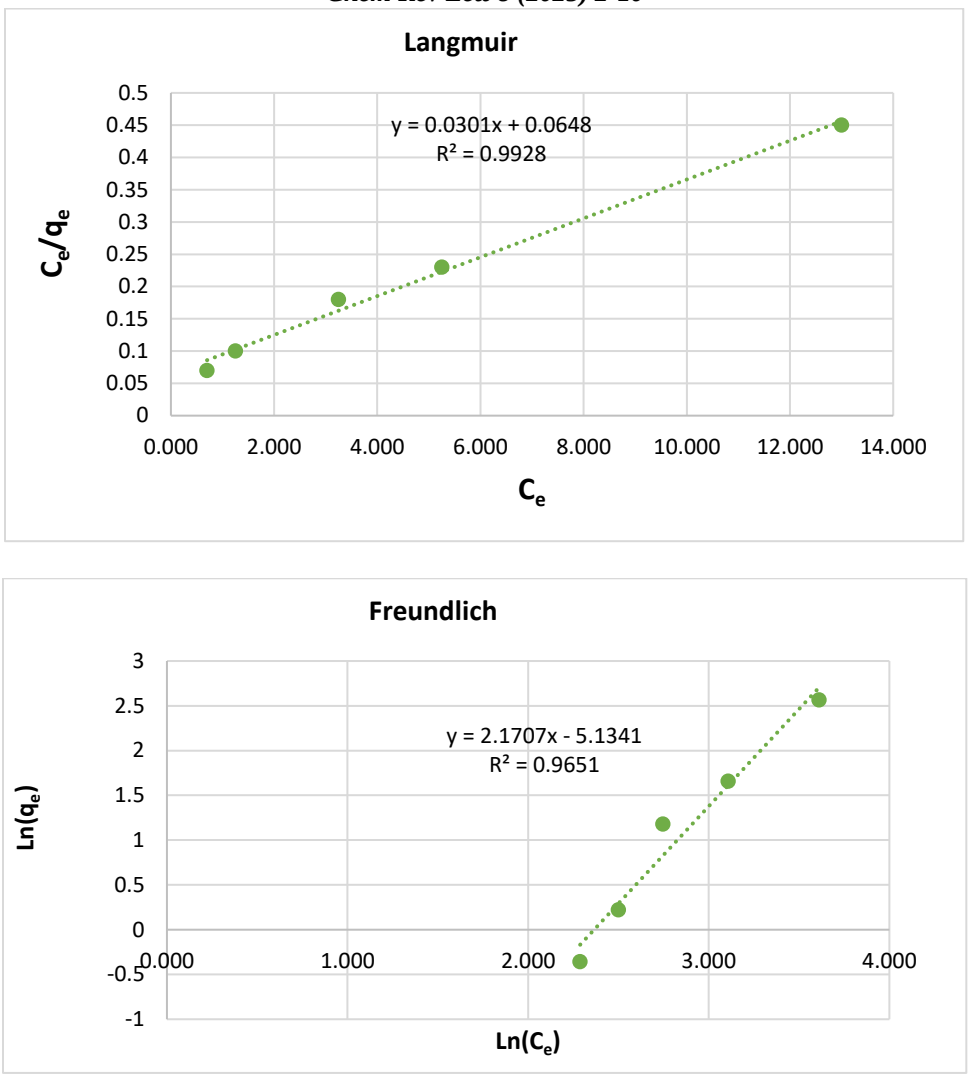

Fig. 9. Adsorption isotherms for the adsorption of CFX onto Fe_3O_4/ZnO@GO

$0.9\lambda/\beta \cos\theta$ used for calculating the average crystallite size of Fe_3O_4/ZnO@GO, where D is the diameter of the nanoparticles, λ (CuKα) =1.5406 Å and β is the full width at half-maximum of the diffraction lines. Also, the CFX and AMX (purity>98%) was purchased from Sigma-Aldrich (Spain). The CFX solution was provided via dissolving 1 g of its powder in methanol and deionized water. The concentrations of CFX and AMX were examined via UV–Vis spectrophotometer (SQ4802; UNICO, Dayton, NJ, USA) at 230 and 278 nm.

Green synthesis of Fe_3O_4/ZnO@GO

The mixture of $FeCl_3.6H_2O$ (1.5 g) and $ZnCl_2$ (1 g) were stirred in water (10 mL). Subsequently, water extract of Petasites hybridus rhizome (5 mL) was added smoothly to previous solution at 100 ºC in round bottom flask and stirred for 5 h. After this time, the mixture temperature was decreased to room temperature and the mixture was sonicated for 30 min and centrifuged at 7000 rpm for about 10 min for deleting the undesired organic compounds and Fe_3O_4/ZnO MNCs was produced in this stage. The produced Fe_3O_4/ZnO MNCs (0.1 g) and GO (0.1 g) were mixed with 100 mL water extract of Petasites hybridus rhizome at 150 ºC for 1 h. By employing centrifuge, the colloid was separated, cleaned with water, dried and was calcinated at 300 ºC for 45 min. The solid was cooled to room temperature and washed several times with mixture of water and ethanol (50:50) and pure Fe_3O_4/ZnO@GO was separated with external magnetic field and dried at room temperature during 24 h.

Adsorption studies

CFX and AMX adsorption tests with 2-20 mg of Fe_3O_4/ZnO@GO MNCs were accomplished in 25 mL stoppered conical flask containing 10 mL of various

concentrations of CFX and AMX solution (10 to 60 mg L^{-1}). The pH of the CFX and AMX solution altered to 2–10 (HCl and NaOH). The mixture of CFX and AMX was stirred in a water bath shaker at various temperature (10, 25, 35, and 45°C) at a fixed speed of 120 rpm for 24 h. Subsequently, all samples were withdrawn at various time and CFX and AMX loaded Fe_3O_4/ZnO@GO was isolated with magnet. Ultimately, the C_e factor for adsorption of CFX and AMX were analyzed via UV–visible spectrophotometry at 230 and 278 nm and q_e factor of adsorption was obtained via Equation (3) and (4):

$$q_{e(CFX)} = \frac{(C_{0(CFX)} - C_{e(CFX)})V\,(CFX)}{W} \quad (3)$$

$$q_{e(AMX)} = \frac{(C_{0(AMX)} - C_{e(AMX)})V\,(AMX)}{W} \quad (4)$$

Where C_0 and C_e (mg L^{-1}) are initial and equilibrium concentrations of CFX and AMX molecules, respectively, V (L) displays volume of standard CFX and AMX solution, and W (g) connects with the mass of Fe_3O_4/ZnO@GO in all tests.

4. Conclusion

In this study, a magnetic graphene was prepared *via* a simple method and it is applied for adsorption of CFX from water. The BET surface area of Fe_3O_4/ZnO@GO was 134.78 m^2g^{-1}. The paramagnetic Fe_3O_4/ZnO@GO provided the advantage of magnetic separation of the adsorbent. The greatest CFX and AMX adsorption capacity was noticed within the equilibrium time 15 min, at pH 6.0 and 8.5 respectively, adsorbent dosage 10 mg and under a temperature of 25°C. The experimental equilibrium data were tested using the isotherms of Langmuir and Freundlich, models.

Acknowledgements

This article is based on the Ph.D. Thesis, Islamic Azad University, Qaemshahr Branch.

References

[1] B. Halling-Sorensen, S.N. Nielsen, P.F. Lanzky, F. Ingerslev, H.C. Lutzhorft, S.E. Jorgensen, Occurence, fate and effects of pharmaceutical substances in the environment a review. Chemosphere 36 (1998)357–393.

[2] Z. Aksu, O. Tunc, Application of biosorption for penicillin G removal: comparison with activated carbon. Process Biochemistry 40 (2005)831–847.

[3] R.E. Alcock, A. Sweetman, K.C. Jones, Assessment of organic contaminant fate in wastewater treatment plants. I. Selected compounds and physicochemical properties. Chemosphere 38 (1999)2247-2262.

[4] M. L. Richardson, J. M. Bowron, The fate of pharmaceutical chemicals in the aquatic environment. Journal of Pharmacy and Pharmacology 37 (1985)1-12.

[5] B. Halling-Sorensen, Algal toxicity of antibacterial agents used in intensive farming. Chemosphere 40 (2000)731–739.

[6] H.C. Holten Lutzhoft, B. Halling-Sorensen, S. E. Jorgensen, Algal toxicity of antibacterial agents applied in Danish fish farming. Archives of Environmental Contamination and Toxicology 36 (1999) 1–6.

[7] X. Pan, C. Deng, D. Zhang, J. Wang, G. Mu, Y. Chen, Toxic effects of amoxicillin on the photosystem II of Synechocystis sp. characterized by a variety of in vivo chlorophyll fluorescence tests. Aquatic Toxicology 89 (2008) 207–213.

[8] J. Rivera-Utrilla, M. Sanchez-Polo, M. A. Ferro-Garcia, G. Prados-Joya, R. Ocampo-Perez, Chemosphere 93(2013)1268.

[9] H. R. Pouretedal and N. Sadegh, J. Water. Process. Eng. 1(2014) 64.

[10] Z. Aksu and O. Tunc, Process. Biochem. 40 (2005) 831.

[11] R. Zandipak, S. Sobhanardakani, Clean. Technol. Environ. Policy. 20(2018)871.

[12] R. Zandipak, S. Sobhan Ardakani, A. Shirzadi, Separ. Sci. Technol. 55(2020)456.

[13] O. Kerkez-Kuyumcu, Ş.S. Bayazit, M.A. Salam, J. Ind. Eng. Chem. 36(2016)198.

[14] S. Zavareh, T. Eghbalazar, J. Environ. Chem. Eng. 5 (2017) 3337.

[15] R. Mostafaloo, M. H. Mahmoudian, M. Asadi-Ghalhari, J. Photochem. Photobiol. A 382,111926 (2019).

[16] P. Manjunatha, Y.A. Nayaka, Chem. Data. Collect. 21(2019)100217.

[17] M. Sheydaei, H.R.K. Shiadeh, B. Ayoubi-Feiz, R. Ezzati, Chem. Eng. J. 353 (2018)138.

[18] a) F. Einollahi Peer, N. Bahramifar, H. Younesi, J. Taiwan. Inst. Chem. Eng. 87(2018)225. b) A. S. Makinta, M. B. Fugu, N. P. Naomi, M. M. Mahmud, A. A. Ahmed, Physicochemical Characterization and Antimicrobial Activity of Mechanochemically and Solvent-Based Synthesized Mn(II) Complexes of Cefixime and Cefuroxime, *Chem. Rev. Lett.* 6 (2022) 261-267.

[19] X. Wang, R. Yin, L. Zeng, M. Zhu, Environ. Pollut. 253 (2019)100.

[20] S.D. Baere, P.D. Backer, Quantitative determination of amoxicillin in animal feed using liquid chromatography with tandem mass spectrometric detection. Analytica Chimica Acta 586 (2007) 319–325.

[21] Z. Aksu, O. Tunc, Application of biosorption for penicillin G removal: comparison with activated carbon. Process Biochemistry 40 (2005)831–847.

[22] R. Andreozzi, M. Canterino, R. Marotta, N. Paxeus, Antibiotic removal from wastewaters: the ozonation of amoxicillin. Journal of Hazardous Materials 122 (2005)243–250.

[23] C. C. Jara, D. Fino, V. Specchia, G. Saracco, P. Spinelli, Electrochemical removal of antibiotic from wastewaters. Applied Catalyst B: Environmental 70 (2007) 479–487.

[24] a) B. Baghernejad, F. Nuhi, A new approach to the facile synthesis of 1,8-dioxooctahydroxanthene using nano-TiO2/

CNT as an efficient catalyst, Chem. Rev. Lett. 6 (2022) 268-277. b) S. Soleimani Amiri, Z. Hossaini, Z. Azizi, Synthesis and investigation of antioxidant and antimicrobial activity of new pyrazinopyrroloazepine derivatives using Fe3O4/CuO/ZnO@MWCNT MNCs as organometallic nanocatalyst by new MCRs, Appl. Organomet. Chem., 36 (2022) e6573. c) S. Soleimani-Amiri, Z. Hossaini, Z. Azizi, Synthesis and Investigation of Biological Activity of New Oxazinoazepines: Application of Fe3O4/CuO/ZnO@MWCNT Magnetic Nanocomposite in Reduction of 4-Nitrophenol in Water, Polycycl. Aromat. Compd., 43 (2022) 2938-2959. d) Z. Hossaini, S. Ahmadi, D. Zareyee, S. Soleimani Amiri, Green synthesis of new spiropyrroloisatin and spiroindenopyrroles using biosynthesized CuO/ZnO@MWCNTs nanocatalyst, Chem. Rev. Lett., (2024) 10.22034/crl.2024.472507.1400. e) M. Sheydaei, M. Edraki, Poly(butylene trisulfide)/CNT nanocomposites: synthesis and effect of CNT content on thermal properties, J. Chem. Lett. 3 (2022) 159-163. f) B. Ghanavati, A. Bozorgian, J. Ghanavati, Removal of Copper (II) Ions from the Effluent by Carbon Nanotubes Modified with Tetrahydrofuran, *Chem. Rev. Lett.* 6 (2022) 68-75.

[25] a) S. Soleimani-Amiri, Z. Hossaini, Z. Azizi, Synthesis and Investigation of Biological Activity of New Oxazinoazepines: Application of Fe3O4/CuO/ZnO@MWCNT Magnetic Nanocomposite in Reduction of 4-Nitrophenol in Water, Polycycl. Aromat. Compd., 43 (2022) 2938-2959. b) S. Soleimani Amiri, Z. Hossaini, Z. Azizi, Synthesis and investigation of antioxidant and antimicrobial activity of new pyrazinopyrroloazepine derivatives using Fe3O4/CuO/ZnO@MWCNT MNCs as organometallic nanocatalyst by new MCRs, Appl. Organomet. Chem., 36 (2022) e6573. c) d) H. Ghavidel, B. Mirza, S. Soleimani-Amiri, A Novel, Efficient, and Recoverable Basic Fe3O4@C Nano-Catalyst for Green Synthesis of 4H-Chromenes in Water via One-Pot Three Component Reactions, Polycycl. Aromat. Compd., 41 (2021) 604-625. e) Z. Samiei, S. Soleimani-Amiri, Z. Azizi, Fe3O4@C@OSO3H as an efficient, recyclable magnetic nanocatalyst in Pechmann condensation: green synthesis, characterization, and theoretical study, Mol. Divers., 25 (2021) 67-86. f) S. Soleimani-Amiri, Y. Salemi, Novel butane sulfonic acid-functionalized core–shell magnetic nanocatalysts for ultrasound-assisted coumarin synthesis, New J Chem., 48 (2024) 2299-2310. g) P. O. Ameh, Synthesized iron oxide nanoparticles from Acacia nilotica leaves for the sequestration of some heavy metal ions in aqueous solutions, *J. Chem. Lett.* 4 (2023) 38-51.

[26] S. Babaee Zadvarzi, A. Akbar Amooey, Environmental Sciences Europe 35 (2023)60.

[27] H.R. Ghorbani, Biological and Non-Biological Methods for Fabrication of Copper Nanoparticles. Chemical Engineering Communications, 202 (2015) 1463–1467.

[28] H.R. Ghorbani. Chemical synthesis of copper nanoparticles, Oriental Journal of Chemistry 30 (2014) 803-806.

[29] H.R. Ghorbani. Biological coating of paper using silver nanoparticles, IET Nanobiotechnology 8(2014)263-266.

[30] A. Marzban, A. Akbarzadeh, M. Shafiee Ardestani, F. Ardestani and M. Akbari, Synthesis of Nano-Niosomal Deferoxamine and Evaluation of its Functional Characteristics to Apply as an Iron-Chelating Agent, The Canadian Journal of Chemical Engineering, 96 (2018)107-112.